PAPER

Operating mode dependent energy transfer efficiency in a quantum well waveguide

IOP Publishing | Astro Ltd Laser Physics

Laser Phys. **33** (2023) 106001 (9pp) https://doi.org/10.1088/1555-6611/acf4e4

Operating mode dependent energy transfer efficiency in a quantum well waveguide

F Al-Dolaimy[1], M H Kzar[2], N Y Jamil[3], M Zaid[4], F A Rasen[5], S Hussain[6,7], K Al-Majdi[8], K S Mohsen[9], A H Alawadi[10,11,12] and A Alsaalamy[13,*]

[1] Al-Zahraa University for Women, Karbala, Iraq
[2] College of Physical Education and Sport Sciences, Al-Mustaqbal University, 51001 Hillah, Babil, Iraq
[3] Department of Radiology & Sonar Techniques, Al-Noor University College, Nineveh, Iraq
[4] Department of biomedical engineering, Al-Manara College for Medical Sciences, Maysan, Iraq
[5] Department of medical engineering, Al-Esraa University College, Baghdad, Iraq
[6] Hybrid Materials Center (HMC), Sejong University, Seoul 05006, Republic of Korea
[7] Department of Nanotechnology and Advanced Materials Engineering, Sejong University, Seoul 05006, Republic of Korea
[8] Department of biomedical engineering, Ashur University College, Baghdad, Iraq
[9] Information and Communication Technology Research Group, Scientific Research Center, Al-Ayen University, Thi-Qar, Iraq
[10] College of technical engineering, The Islamic University, Najaf, Iraq
[11] College of technical engineering, The Islamic University of Al Diwaniyah, Al-Qadisiyah, Iraq
[12] College of technical engineering, The Islamic University of Babylon, Hillah, Iraq
[13] College of technical engineering, Imam Ja'afar Al-Sadiq University, Al-Muthanna 66002, Iraq

E-mail: alihashimalsalamy78@gmail.com

Received 15 August 2023
Accepted for publication 26 August 2023
Published 7 September 2023

Abstract

In this paper, we delve into the intricate interplay between optical fields with varying relative phases in a closed-loop configuration semiconductor quantum well waveguide with four distinct energy levels, and how it impacts the Fraunhofer diffraction patterns obtained via four-wave mixing. By harnessing a strong control field, a standing wave driving field, and two weak probe and signal fields, we drive the waveguide to generate these patterns with maximum efficiency. To achieve this, we consider three distinct light-matter interaction scenarios, where the system is first set up in either a lower electromagnetically induced transparency or a coherent population trapping state, followed by a final state that enables electron spin coherence (ESC) induction. Our results reveal that the efficiency of Fraunhofer diffraction in the quantum well waveguide can be enhanced significantly under specific parameter regimes via the spin coherence effect. Further investigation of the light-matter interaction in the ESC zone, where only one of the control fields is a standing wave field, demonstrates that spin coherence facilitates more efficient transfer of energy from the probe light to the third and fourth orders, highlighting its crucial role in shaping the diffraction patterns.

* Author to whom any correspondence should be addressed.

Keywords: electromagnetically induced grating, electron spin coherence, quantum well waveguide

(Some figures may appear in colour only in the online journal)

1. Introduction

Electromagnetically induced transparency (EIT) is a fascinating quantum optics phenomenon that occurs when a strong coupling field interferes with a weak probe field, causing its absorption to vanish [1]. This effect has found applications in numerous domains, including optical bistability [2, 3], enhanced Kerr nonlinearity [4], and optical solitons [5, 6], four-wave mixing (FWM) [7, 8] and so on [9–13].

When a standing-wave (SW) coupling field is applied to an EIT system, it creates an intriguing phenomenon known as electromagnetically induced grating (EIG) [14]. The EIG results in the spatial periodicity of the absorption and dispersion of a traveling wave (TW) probe field. This spatially periodic grating has opened up new possibilities for optical switching [15] and the storage of light that has passed through an atomic medium [16]. The EIG phenomenon can be further understood as a manifestation of the interference between the SW coupling field and the TW probe field, which leads to a modulation in the refractive index of the medium. This modulation gives rise to a spatial grating structure that results in a spatially varying absorption and dispersion.

The potential of EIT and EIG in modern applications has attracted a significant amount of research attention, with a focus on improving the efficiency and understanding the underlying physics. The discovery of EIT and EIG phenomena has been a crucial step towards the development of efficient and advanced optical technologies. Further exploration and development of these phenomena are necessary to continue pushing the boundaries of modern optics.

A wealth of research has been conducted on various multi-level atomic systems that integrate with the original EIG scheme [17–25]. These studies have also delved into more complex four-level configurations that involve interactions with multiple fields, including N-type [26], Ladder-type atomic systems [27], and intriguing processes that occur near plasmonic nanostructures [28] and quantum wells [29]. Such recent works have broadened the horizon of exploring the rich physics of EIT and EIG, paving the way for further investigations.

Quantum coherence phenomena in semiconductors have also been the subject of extensive research. In particular, quantum structures such as quantum dots or wells have demonstrated the ability to control the band gap by altering their geometry [30–34]. This feature makes these structures highly customizable, serving as artificial atoms with potential applications in optoelectronics and quantum information technology. Coherent population trapping (CPT) is another fascinating effect that arises from preparing media in a coherent superposition of ground or metastable states, commonly referred to as dark states [35]. This effect arises due to quantum interference in a three-level system. The same experimental setup used for studying EIT can be utilized for investigating CPT, which requires satisfying the two-photon resonance condition.

Semiconductors have been shown to exhibit EIT through intersubband transitions [36], electron spin coherence (ESC) in a quantum well waveguide [37–42], and nonradiative quantum coherences [39]. Such quantum coherence can be harnessed to observe various quantum phenomena in semiconductors, such as gain without inversion, coherent control of absorption and dispersion, and FWM, all made possible by intersubband optical transitions [43–51].

The objective of this study is to investigate a closed-loop configuration consisting of a four-level medium interacting with four light beams. This configuration is similar to the methods proposed in [46] and can be represented geometrically as a double-V or double Λ-structure due to the symmetry attained by the levels and beams. We explore and compare three distinct scenarios in this system. In the first two cases, the system is initially populated in a lower EIT-state or a CPT superposition state. In the third instance, the system is prepared in a higher state that allows for the induction of ESC.

The results of this study show that the ESC induced in the third scenario produces a highly efficient Fraunhofer diffraction pattern. This phenomenon arises due to FWM processes in the quantum well waveguide. The Fraunhofer diffraction pattern is a result of the interference between the scattered waves and provides important insights into the system's behavior. The efficiency of this pattern is enhanced by the presence of ESC, which amplifies the FWM process.

These findings demonstrate the potential of using ESC in conjunction with FWM processes to achieve highly efficient Fraunhofer diffraction patterns. This study provides insights into the behavior of the closed-loop configuration in various scenarios and highlights the importance of ESC in achieving these results. The findings could be useful in the development of new optical devices and technologies.

1.1. Waveguide model and quantum equations

In this study, we examine a waveguide with multiple quanta wells at four energy levels, as previously investigated by Asadpour *et al* [46]. The energy level diagram and dipole-allowed transitions are illustrated in figure 1. By utilizing the dipole and rotating wave approximations, the Hamiltonian can be expressed in the interaction picture

$$\begin{aligned} \mathrm{H}_{\mathrm{int}}^{I}/\hbar = {} & \Delta_1 |b\rangle\langle b| + \Delta_- |c\rangle\langle c| + (\Delta_- - \Delta_2) |d\rangle\langle d| \\ & - (\Omega_- |a\rangle\langle b| + \Omega_+ |d\rangle\langle b| + \mathrm{H.c}) \\ & - (\Omega_1 |a\rangle\langle b| + \Omega_2 |d\rangle\langle c| + \mathrm{H.c}). \end{aligned} \tag{1}$$

The detunings are defined as $\Delta_1 = \omega_1 - \omega_{ab}$, $\Delta_- = \omega_- - \omega_{ac}$ and $\Delta_2 = \omega_2 - \omega_{dc}$, where $\omega_{mn} = (\varepsilon_m - \varepsilon_n)/\hbar\,[m,n = a,b,c,d; m \neq n, \varepsilon_{m(n)}$ is the energy of state

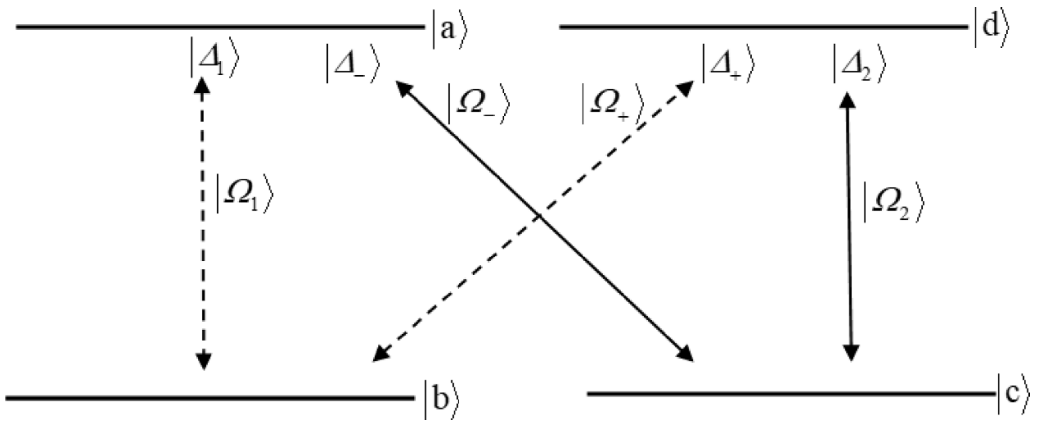

Figure 1. Multiple quantum well waveguide interacts with four laser fields.

$[m(n)]$, $\omega_j(j=1,2,\pm)$ is the frequency of the corresponding laser, and $\Omega_+ = (\vec{\mu}_{bd}.\vec{e}_+)E_+/\hbar$, $\Omega_- = (\vec{\mu}_{ac}.\vec{e}_-)E_-/\hbar$, , $\Omega_1 = (\vec{\mu}_{ab}.\vec{e}_1)E_1/\hbar$, and $\Omega_+ = (\vec{\mu}_{dc}.\vec{e}_+)E_2/\hbar$, are the corresponding Rabi frequencies with $\vec{\mu}_{mn}$ being the dipole moment for the relevant transition $|m\rangle \leftrightarrow |n\rangle, E_j(j=\pm,1,2)$ indicating the corresponding electric field amplitude and $\vec{e}_j$ representing the polarization unit vector of the electric field. The density matrix elements represent the populations and coherences of the quantum states in the system. They can be written as follows:

$$\begin{aligned}
\dot{\rho}_{ab} &= i(\Delta_1 + i\gamma_1)\rho_{ab} + i\Omega_1(\rho_{bb} - \rho_{aa}) + i\Omega_-\rho_{cb} - i\Omega_+\rho_{ad} \\
\dot{\rho}_{bc} &= i[(\Delta_- - \Delta_1) + i\gamma_{dc}]\rho_{bc} - i\Omega_-\rho_{ba} - i\Omega_2\rho_{bd} + i\Omega_+^*\rho_{dc} \\
&\quad + i\Omega_1^*\rho_{ac} \\
\dot{\rho}_{bd} &= i[(\Delta_- - \Delta_2 - \Delta_1) + i\gamma_2]\rho_{bd} + i\Omega_+^*(\rho_{dd} - \rho_{bb}) \\
&\quad - i\Omega_2^*\rho_{bc} + i\Omega_1^*\rho_{ad} \\
\dot{\rho}_{ac} &= i(\Delta_- + i\gamma_3)\rho_{ac} + i\Omega_-(\rho_{cc} + \rho_{aa}) - i\Omega_2\rho_{ad} + i\Omega_1\rho_{bc}
\end{aligned} \tag{2}$$

where $\gamma_i(i=1-3)$ denotes the total dephasing rates that are added phenomenologically, and γ_{dc} denotes the decoherence term between ground states $|b\rangle$ and $|c\rangle$.

1.1.1. EIT case. The proposed scheme utilizes a combination of two Λ-configured EIT subsystems. The first subsystem is formed by a weak probe field with a Rabi frequency of Ω_1 and a strong control field with a Rabi frequency of Ω_-. The second subsystem is formed by another weak probe field with a Rabi frequency of Ω_+ and a strong field with a Rabi frequency of Ω_2.

To solve equation (2), we apply perturbation theory to describe FWM and consider the system in a steady-state condition. This allows us to represent the off-diagonal matrix element $\rho_{ab}^{(1)}$ in terms of the weak probe fields and strong control fields. Specifically, we assume that both probe fields are much weaker than the control fields, so that all atoms remain in the ground state. Using this assumption, we can obtain an expression for $\rho_{ab}^{(1)}$ that takes into account the FWM pathway from level $|b\rangle \rightarrow |a\rangle \rightarrow |c\rangle \rightarrow |d\rangle \rightarrow |b\rangle$.

$$\begin{aligned}
\rho_{ab}^{(1)} &= \frac{-i(\Delta_{cb}\Delta_{ab} + |\Omega_2|^2)\Omega_1}{\Delta_{ab}(\Delta_{cb}\Delta_{db} + |\Omega_2|^2) + \Delta_{db}|\Omega_-|^2} \\
&\quad + \frac{+i\Omega_-\Omega_2^*\Omega_+}{\Delta_{ab}(\Delta_{cb}\Delta_{db} + |\Omega_2|^2) + \Delta_{db}|\Omega_-|^2},
\end{aligned} \tag{3}$$

where $\Delta_{ab} = i(\Delta_1 + i\gamma_1)$, $\Delta_{cb} = i[(\Delta_- - \Delta_1) + i\gamma_{dc}]$, and $\Delta_{db} = i[(\Delta_- - \Delta_2 - \Delta_1) + i\gamma_2]$.

Note that the second term in equation (3) corresponds to the contribution of FWM processes in the medium.

Moving forward, we now turn our focus to the equations of motion that describe the system under the CPT condition.

1.1.2. CPT case. This section deals with a scenario in which the weak probe and signal lights are denoted by Ω_1 and Ω_+, respectively, and the atoms remain in a CPT state

$$\begin{aligned}
|D\rangle &= c_b|b\rangle - c_c|c\rangle, c_b = \frac{\Omega_2}{\sqrt{|\Omega_2|^2 + |\Omega_-|^2}}, \\
c_c &= \frac{\Omega_-}{\sqrt{|\Omega_2|^2 + |\Omega_-|^2}}.
\end{aligned} \tag{4}$$

As a result, a pair of weak probe pulses can propagate through the medium, interacting with the upper legs of the double-Λ scheme in a coherent manner. Given the aforementioned conditions, we can derive the coherence terms as follows:

$$\rho_{bc}^{(1)} = \frac{-i|c_b|^2\Omega_1 + ic_c c_b^*\Omega_+}{\Delta_{ab}}. \tag{5}$$

The presence of the generating field Ω_+ is reflected in the appearance of the term $c_c c_b^*$ in equation (5).

1.1.3. ESC case. We will now consider a scenario in which the system is initially prepared in level $|a\rangle$, and weak probe and signal lights Ω_- and Ω_1 propagate through a medium coherently prepared by the upper legs of a double-Λ scheme. Via the FWM setup in pathway $|a\rangle \rightarrow |c\rangle \rightarrow |d\rangle \rightarrow |b\rangle \rightarrow |a\rangle, \Omega_1$ is generated, with both probe and signal lights Ω_1 and Ω_- being

much weaker than the control fields Ω_+ and Ω_2. The resulting probe susceptibility can be expressed in terms of the relevant density matrix element

$$\rho_{ab}^{(1)} = \frac{i\Omega_+\Omega_2^*\Omega_- + i(\Delta_{ac}\Delta_{ad} + |\Omega_2|^2)\Omega_1}{\Delta_{ab}\Delta_{ac}\Delta_{ad} + \Delta_{ac}|\Omega_+|^2 + \Delta_{ab}|\Omega_2|^2} \tag{6}$$

where, we have:

$$\Delta_{ab} = i(\Delta_1 + i\gamma_1), \tag{7a}$$

$$\Delta_{_{ac}} = i[\Delta_- + i\gamma_3], \tag{7b}$$

$$\Delta_{\mathrm{ad}} = \mathrm{i}[(\Delta_- - \Delta_2) + \mathrm{i}\gamma_5]. \tag{7c}$$

2. Fraunhofer diffraction; patterns in the far field

The Maxwell wave equation can be applied to estimate the diffraction pattern of the probe light in an atomic system by approximating the slowly varying envelope in the steady state regime. This is illustrated below:

$$\frac{\partial E_p}{\partial z} = \frac{ik_p}{2\varepsilon_0}P(\omega_{ij}), \tag{8}$$

orr

$$\frac{\partial E_p}{\partial z'} = \{-\mathrm{Im}(\rho_{ij}) + i\,\mathrm{Re}(\rho_{ij})\}\,E_{\mathrm{probe}}, \tag{9}$$

where $z' = (N\mu_{ij}^2/2\hbar\varepsilon_0)k_p z$ and the unit for z is represented by $k_p = 2\pi/\lambda$, $(N\mu_{ij}^2/2\hbar\varepsilon_0)k_p$.

The transmission function for an atomic sample of interaction length L can be normalized and expressed as

$$T(x) = \exp(-\mathrm{Im}(\rho_{ij})L)\exp(\mathrm{i}\,\mathrm{Re}(\rho_{ij})L). \tag{10}$$

Here, the symbol ρ_{ij} corresponds the susceptibility of the probe beam and can be utilized for analyzing the transmission function.

In equation (10), the initial exponential term pertains to the amplitude while the second term represents the phase modulations. The Fourier transform of the equation yields the Fraunhofer or far-field diffraction equation:

$$J_p(\theta_x) = |F(\theta_x)|^2\,\frac{\sin^2(M\pi\, x\sin\theta_x)}{M^2\sin^2(\pi\, x\sin\theta_x)} \tag{11}$$

where

$$F(\theta_x) = \int_0^1 T(x)\exp(-i2\pi\, x\sin\theta_x)\mathrm{d}x. \tag{12}$$

In the above equation, θ_x represents the diffraction angle in relation to the z direction, while M corresponds to the number of spatial periods of the grating that is being illuminated by the probe beam.

3. Results and analysis of findings

In this section, we will analyze the Fraunhofer diffraction patterns for three distinct physical states: EIT, CPT, and ESC modes. We will consider the control field Ω_2 as a standing wave ($\Omega_2(x) = \Omega_{02}\sin(\pi x/\Lambda_x)$) to investigate the behavior of diffraction under the same control parameters. Our aim is to highlight the significant differences in the Fraunhofer diffraction patterns for each mode.

The amplitude diagrams for EIT, CPT, and ESC modes are shown in figure 2(a), illustrating the amplitude diagram in terms of the x parameter. We notice that all three cases exhibit an oscillatory behavior. However, the amplitude diagram for the EIT mode reaches its maximum at the antinodes of the SW, while for both CPT and ESC modes, the amplitude diagram drops to zero at the antinodes of the standing wave. Interestingly, we observe that the intensity of the EIT mode is significantly higher than that of the other modes, indicating that most of the probe energy remains in the zero-order diffraction.

The behavior of the patterns in CPT and ESC modes is quite similar in terms of size, which implies that they share some common features. Nevertheless, the phase diagram of the transmission function in figure 2(b) reveals a notable difference. We observe that the value of the phase diagram in the ESC mode is considerably higher than that of the other modes, indicating that some of the probe energy may transfer to higher orders. In contrast, the intensity of the phase diagram in the CPT mode reaches zero at some points (nodes of the SW).

Such diagrams provide valuable insights into the behavior of EIT, CPT, and ESC modes. The amplitude diagram highlights the significant differences in the diffraction patterns, with the EIT mode exhibiting a significantly higher intensity than the other modes. Moreover, the phase diagram emphasizes the importance of considering the physical state when examining diffraction patterns, as it reveals the possibility of energy transfer to higher orders in the ESC mode.

Figure 3 displays the Fraunhofer diffraction pattern for the parametric conditions in figure 2. The solid line represents the EIT mode, which shows that most of the probe energy is collected in the zeroth order, and only a small amount of the probe energy is transferred to the first order. On the other hand, in the CPT (dashed) and ESC (dotted) modes, some of the probe energy is transferred to higher diffraction orders. Nonetheless, in these cases, the energy collected in the zero order is still more than that in the higher orders.

In the next step, we aim to identify conditions where the energy of the probe field is transferred significantly beyond the Fraunhofer diffraction pattern. As illustrated in figure 1, the FWM phenomenon causes the applied fields' shape to form a closed loop. Therefore, the relative phase of the applied fields can affect the quantum well's optical properties. This

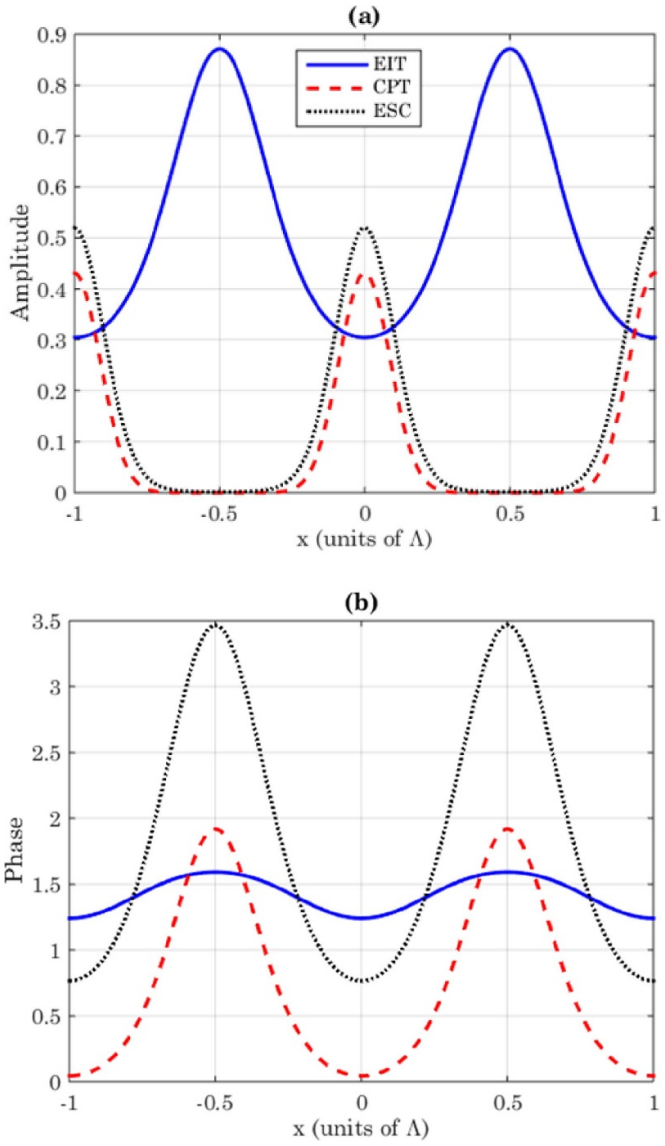

Figure 2. Amplitude (a) and phase (b) diagram versus parameter x in EIT (solid), CPT (dashed) and ESC (dotted) lines. The selected parameters are $\gamma_1 = \gamma_2 = 1, \gamma_{dc} = 0.01, \Delta_1 = \Delta_- = \Delta_2 = 0$, $\Omega_{02} = \Omega_- = 1$ (EIT), $\gamma_1 = 1, \Delta_1 = 0, \Omega_{02} = \Omega_- = 1$ (CPT) and $\gamma_1 = \gamma_3 = 1, \gamma_5 = 0.001, \Delta_1 = \Delta_- = \Delta_2 = 0, \Omega_{02} = \Omega_+ = 1$ (ESC).

is expressed by equations (3), (5) and (6), which are given below:

$$\rho_{ab}^{(1)} = \frac{-i(\Delta_{cb}\Delta_{ab} + |\Omega_2|^2)\Omega_1}{\Delta_{ab}(\Delta_{cb}\Delta_{db} + |\Omega_2|^2) + \Delta_{db}|\Omega_-|^2} + \frac{+i\Omega_-\Omega_2^*\Omega_+ \exp(i\varphi)}{\Delta_{ab}(\Delta_{cb}\Delta_{db} + |\Omega_2|^2) + \Delta_{db}|\Omega_-|^2} \quad (13)$$

$$\rho_{bc}^{(1)} = \frac{-i|c_b|^2\Omega_1 + ic_c c_b^*\Omega_+ \exp(i\varphi)}{\Delta_{ab}} \quad (14)$$

$$\rho_{ab}^{(1)} = \frac{i\Omega_+\Omega_2^*\Omega_- \exp(i\varphi) + i(\Delta_{ac}\Delta_{ad} + |\Omega_2|^2)\Omega_1}{\Delta_{ab}\Delta_{ac}\Delta_{ad} + \Delta_{ac}|\Omega_+|^2 + \Delta_{ab}|\Omega_2|^2}. \quad (15)$$

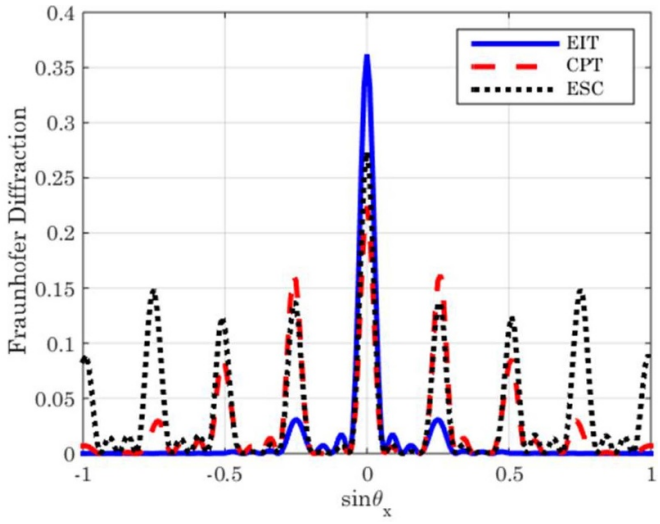

Figure 3. Fraunhofer diffraction pattern versus $\sin(\theta_x)$ in EIT (solid), CPT (dashed) and ESC (dotted) lines. The selected parameters are same as figure 2.

These relationships show that the phase of the control fields plays a crucial role in determining the optical properties of the quantum well. By manipulating the relative phase of the applied fields, we can potentially achieve significant energy transfer beyond the Fraunhofer diffraction limit.

In figure 4, the amplitude (a) and phase (b) diagrams of the transmitted field are shown for the case where the relative phase of the applied fields is $\varphi = \pi/4$. It is observed that the intensity of the amplitude modulation for all three modes has decreased compared to figure 2. Additionally, the amplitude modulation for the ESC mode (dotted line) has the lowest value compared to the EIT and CPT modes. On the other hand, the phase curve of the transmission function has increased significantly compared to figure 2(b).

Therefore, it is expected that in these conditions, the intensity of Fraunhofer diffraction in higher orders is greater than the zero order. The Fraunhofer diffraction curves for the parametric conditions of figure 4 for different states (EIT, CPT and ESC) are shown in figure 5. For the EIT mode (solid line), the value of the probe energy in the zero order is higher than the first and second orders, but the value of the probe energy in the third order is higher than the other orders. For the CPT mode (dashed line), the amount of probe energy in the first order is almost zero, and most of the energy amount has been transferred to the second order. The best conditions for the ESC mode (dotted line) occur so that the maximum amount of probe field energy is transferred to the third and fourth orders. In this case, the minimum amount of energy of the probe field is collected in the zeroth order.

Figure 6 illustrates the different orders of Fraunhofer diffraction in terms of Ω_{02} for relative phase $\varphi = 0$ (a) and $\varphi = \pi/4$ (b) for the EIT condition. For $\varphi = 0$, most of the energy of the probe field is accumulated in the zeroth order, and very little energy is transferred to the first order. The energy of other orders is zero. For the case of $\varphi = \pi/4$ (b), it is observed that for different intensities, some of the probe energy is transferred

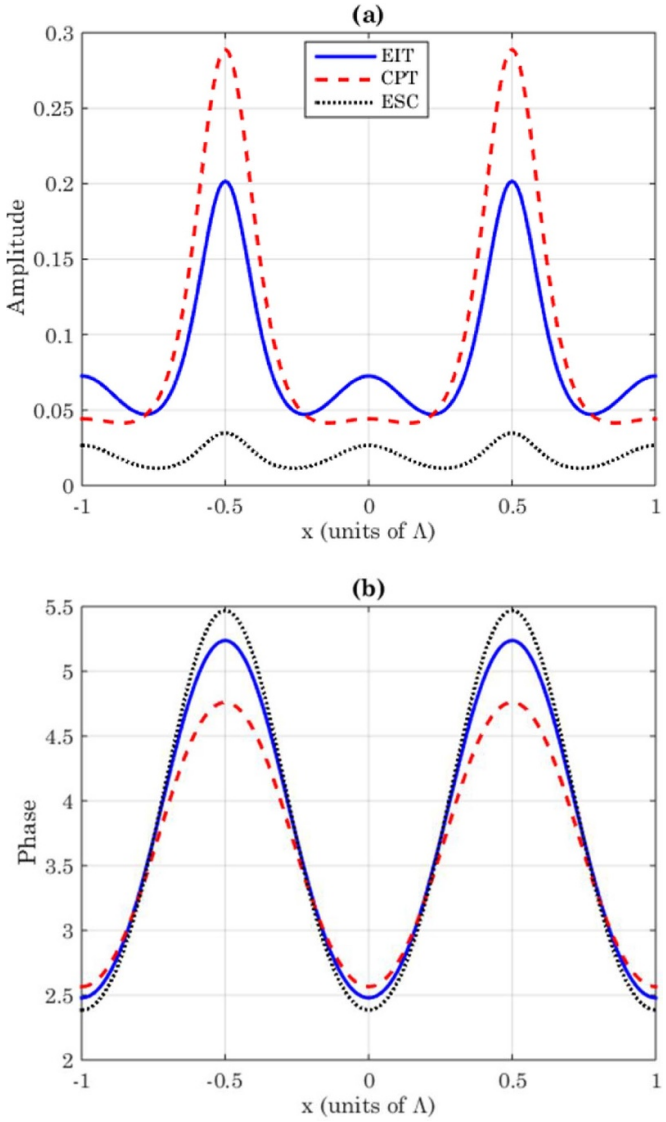

Figure 4. Amplitude (a) and phase (b) diagram versus parameter x in EIT (solid), CPT (dashed) and ESC (dotted) lines for relative phase $\varphi = \pi/4$. The selected parameters are same as figure 2.

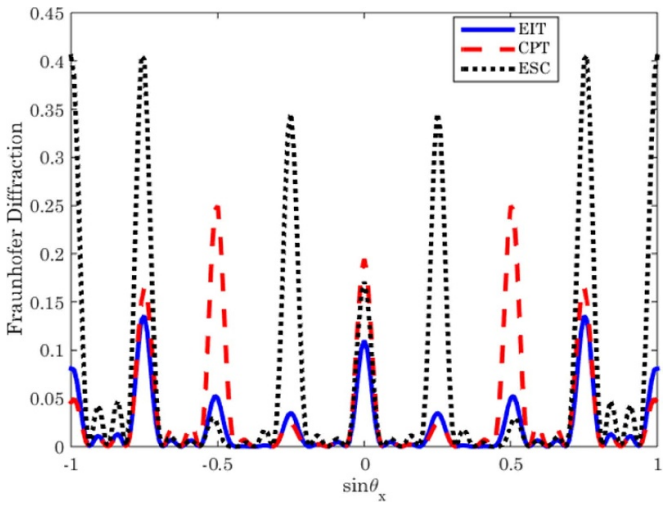

Figure 5. Fraunhofer diffraction pattern versus $\sin(\theta_x)$ in EIT (solid), CPT (dashed) and ESC (dotted) lines for relative phase $\varphi = \pi/4$. The selected parameters are same as figure 2.

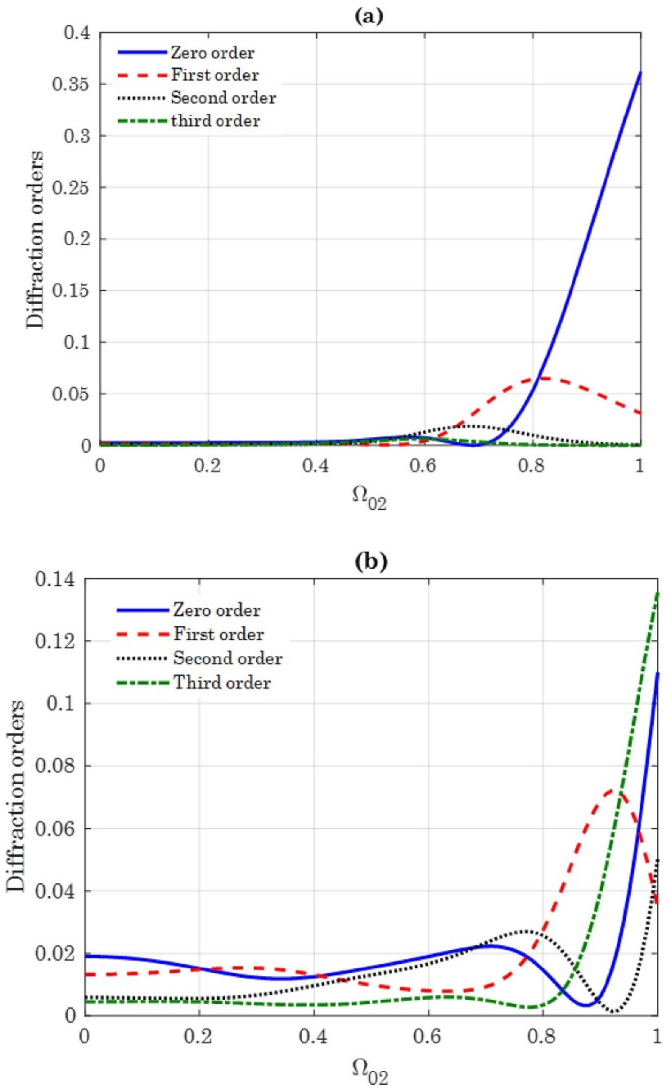

Figure 6. Different diffraction orders versus parameter Ω_{02} in EIT condition for relative phase $\varphi = 0$ (a) and $\varphi = \pi/4$ (b). The selected parameters are same as EIT conditions in figure 2.

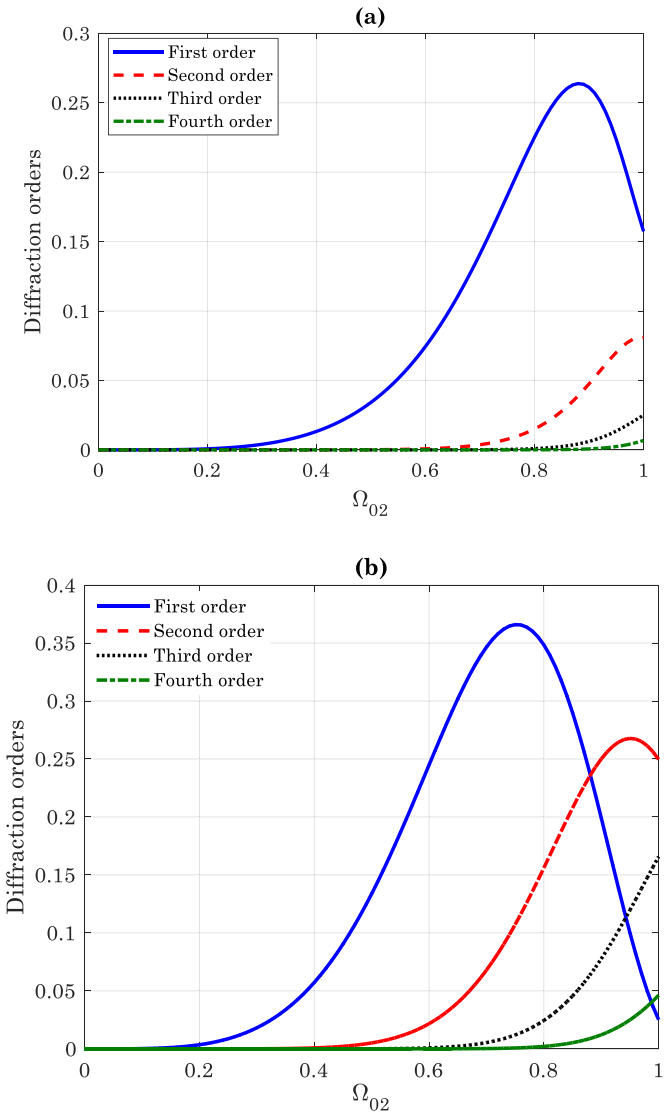

Figure 7. Different diffraction orders versus parameter Ω_{02} in CPT condition for relative phase $\varphi = 0$ (a) and $\varphi = \pi/4$ (b). The selected parameters are same as CPT conditions in figure 2.

to different diffraction orders. For $\Omega_{02} = 0.88$, most of the probe energy accumulates in the first order, but for $\Omega_{02} = 1$, the largest amount of probe energy accumulates in the third order. Therefore, it is possible to control the energy transfer of the probe field in different orders by controlling the intensity of the control field.

In figure 7, we present the diffraction orders for the CPT mode as a function of Ω_{02} and for the relative phase for two different regimes values $\varphi = 0$ (a) and $\varphi = \pi/4$ (b). In panel (a) and for $\varphi = 0$, the majority of the probe energy is concentrated in the first order, with only a small fraction being transferred to higher orders. As we move to panel (b) for $\varphi = \pi/4$ and reduce the intensity of the coupling field, the probe energy in all diffraction orders is significantly reduced. However, as we increase the intensity of the coupling field Ω_{02}, the probe energy in higher diffraction orders starts to increase. For a coupling field intensity of $\Omega_{02} = 1$, the majority of the probe energy is transferred to the second order, while the energy of the third order is greater than that of the first order. These results demonstrate the significant impact of the relative phase and the coupling field intensity on the energy transfer between diffraction orders.

The different diffraction orders versus the Rabi frequency Ω_{02} in ESC mode for two relative phase values $\varphi = 0$ (a) and $\varphi = \pi/4$ (b) are presented in figure 8. For the relative phase $\varphi = 0$, it can be observed that as the intensity of the Rabi frequency increases, most of the probe energy is collected in the first order. However, for very large Rabi frequencies up to $\Omega_{02} = 1$, the intensity of the second order is higher than the other orders. Finally, for $\Omega_{02} = 1$, most of the probe energy is accumulated in the third order. In part (b) of figure 8, most of the probe energy is transferred to the higher orders when the Rabi frequency intensity of the coupling field is equal to $\Omega_{02} \simeq 0.7$. In this case, the maximum energy of the probe

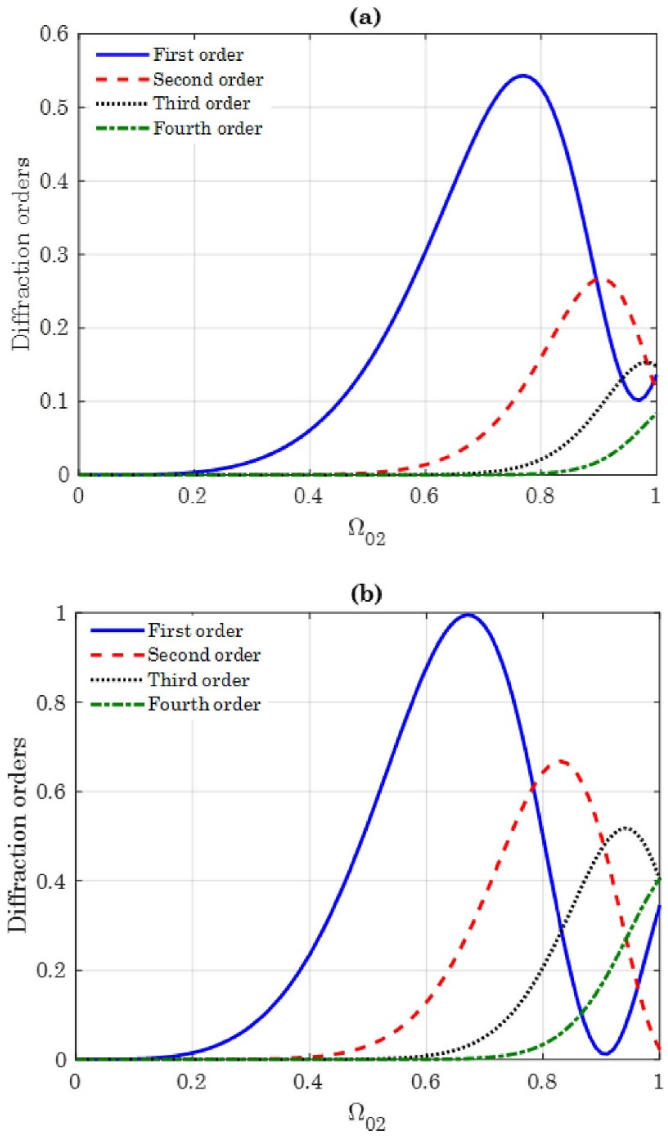

Figure 8. Different diffraction orders versus parameter Ω_{02} in ESC condition for relative phase $\varphi = 0$ (a) and $\varphi = \pi/4$ (b). The selected parameters are same as ESC conditions in figure 2.

field is placed in the first order. However, for the $\Omega_{02} = 1$, most of the probe energy is transferred to the third and fourth orders, respectively. The results suggest that, in ESC conditions, there is a better possibility of transmitting the probe energy to the higher diffraction orders with greater efficiency compared to EIT and CPT conditions. Comparing the results obtained for these different modes, it can be concluded that the ESC mode is more efficient in transferring the probe energy to the higher diffraction orders compared to the EIT and CPT modes.

These results highlight the importance of the choice of the operating mode in determining the efficiency of energy transfer to different diffraction orders. By selecting the ESC mode, it is possible to achieve a higher efficiency in transferring the probe energy to the higher diffraction orders, which can have significant applications in various areas, including optical communication, imaging, and sensing.

4. Conclusion

In this study, we have investigated the influence of relative phase differences between applied lights on the Fraunhofer diffraction pattern in a quantum well waveguide structure composed of two V-type configurations. We have focused on three different interaction regimes: EIT, CPT, and ESC. In the CPT scenario, the system is trapped in a superposition of two lower ground states, while in the EIT regime, it is initially prepared at a lower ground level. However, in the ESC regime, we prepared the system in a higher excited state.

Our findings suggest that the ESC interaction regime leads to an increase in diffraction efficiency. We have shown that for this regime, it is possible to transmit the probe energy to higher diffraction orders with greater efficiency compared to EIT and CPT conditions. Our study highlights the importance of carefully choosing the interaction regime to achieve efficient and controlled manipulation of light in quantum well waveguide structures. Overall, this work provides insights into the role of FWM processes in controlling the propagation of light in complex optical systems.

Acknowledgments

The author K M Batoo would like to thank Researchers Supporting Project No. (RSP2023R148), King Saud University, Riyadh, Saudi Arabia for the financial support.

References

[1] Wu Y and Yang X 2005 *Phys. Rev.* A **71** 053806
[2] Asadpour S H and Rahimpour Soleimani H 2016 *J. Appl. Phys.* **119** 023102
[3] Solookinejad G, Jabbari M, Nafar M, Ahmadi E and Asadpour S 2018 *J. Appl. Phys.* **124** 063102
[4] van Doai L, Le Thuy An N, Xuan Khoa D, Sau V N and Huy Bang N 2019 *J. Opt. Soc. Am.* B **36** 2856
[5] Wu Y and Deng L 2004 *Phys. Rev. Lett.* **93** 143904
[6] Wu Y 2005 *Phys. Rev.* A **71** 053820
[7] Wu Y and Yang X 2007 *Phys. Rev.* B **76** 054425
[8] Wu Y 2008 *J. Appl. Phys.* **103** 104903
[9] Asadpour S H, Nasehi R, Soleimani H R and Mahmoudi M 2015 *Superlattices Microstruct.* **85** 112–23
[10] Asadpour S H, Hamedi H R and Jafari M 2018 *Appl. Opt.* **57** 4013–9
[11] Liu S, Liu S, Zhu Z and Yang W-X 2016 *Laser Phys.* **26** 035401
[12] Feng Y *et al* 2022 *IEEE Trans Terahertz Sci. Technol.* **12** 678–81
[13] Shui T, Yang W-X, Zhang Q, Liu X and Li L 2019 *Phys. Rev.* A **99** 013806
[14] Ling H Y, Li Y-Q and Xiao M 1998 *Phys. Rev.* A **57** 1338
[15] Brown A W and Xiao M 2005 *Opt. Lett.* **30** 699–701
[16] Tabosa J and Lezama A 2007 *J. Phys. B: At. Mol. Opt. Phys.* **40** 2809
[17] Guo R *et al* 2023 *Photonics Res.* **11** 189–95
[18] Zhao Q *et al* 2022 *Appl. Opt* **61** 7225–30
[19] Xiao Z-H, Shin S G and Kim K 2010 *J. Phys. B: At. Mol. Opt. Phys.* **43** 161004
[20] Carvalho S A and de Araujo L E 2011 *Phys. Rev.* A **83** 053825
[21] Zhang Y, Wang Z, Nie Z, Li C, Chen H, Lu K and Xiao M 2011 *Phys. Rev. Lett.* **106** 093904

[22] Kuang S-Q and Yang H-G 2013 *J. Opt. Soc. Am.* B **30** 136–9
[23] Cheng G-L, Zhong W-X and Chen A-X 2015 *Opt. Express* **23** 9870–80
[24] Chen Y-Y, Liu Z-Z and Wan R-G 2017 *Appl. Opt.* **56** 5736–44
[25] Liu Y-M, Gao F, Fan C-H and Wu J-H 2017 *Opt. Lett.* **42** 4283–6
[26] Naseri T and Sadighi-Bonabi R 2014 *J. Opt. Soc. Am.* B **31** 2430–7
[27] Bibhas K D and Prasanta K M 2006 *J. Phys. B: At. Mol. Opt. Phys.* **39** 1145
[28] Asadpour S H, Kirova T, Hamedi H R, Yannopapas V and Paspalakis E 2023 *Eur. Phys. J. Plus* **138** 246
[29] Vafafard A, Sahrai M, Hamedi H R and Asadpour S H 2020 *Sci. Rep.* **10** 1–10
[30] Zhao Q *et al* 2022 *Micromachines* **13** 826
[31] Zhang B *et al* 2023 *J. Phys. D: Appl. Phys.* **56** 365502
[32] Jabbari M 2017 *Eur. Phys. J. Plus* **132** 244
[33] You Y, Qi Y-H, Niu Y-P and Gong S-Q 2019 *J. Phys.: Condens. Matter* **31** 105801
[34] Chen H-J 2020 *Laser Phys. Lett.* **17** 025201
[35] Kirova T, Jia N, Asadpour S H, Qian J, Juzeliūnas G and Hamedi H R 2020 *Opt. Lett.* **45** 5440–3
[36] Phillips M and Wang H 2002 *Phys. Rev. Lett.* **89** 186401
[37] Yang X-X, Li Z-W and Wu Y 2005 *Phys. Lett.* A **340** 320–5
[38] Asadpour S H and Soleimani H R 2014 *Opt. Commun.* **315** 394–8
[39] Liu J-B, Liu N, Shan C-J, Liu T-K and Huang Y-X 2010 *Phys. Rev.* E **81** 036607
[40] Asadpour S H, Jaberi M and Soleimani H R 2013 *J. Opt. Soc. Am.* B **30** 1815
[41] Gurudev Dutt M V, Cheng J, Wu Y, Xu X, Steel D G, Bracker A S, Gammon D, Economou S E, Liu R-B and Sham L J 2006 *Phys. Rev.* B **74** 125306
[42] Phillips M C and Wang H 2004 *Phys. Rev.* B **69** 115337
[43] Wang Z and Yu B 2018 *Plasmonics* **13** 567–74
[44] Kosionis S G 2018 *Superlattices Microstruct.* **118** 152–9
[45] Naseri T and Daneshfar N 2018 *J. Theor. Appl. Phys.* **12** 183–9
[46] Asadpour S H, Faizabadi E, Kudriašov V, Paspalakis E and Hamedi H 2021 *Eur. Phys. J. Plus* **136** 1–13
[47] Asadpour S H, Kirova T, Qian J, Hamedi H R, Juzeliūnas G and Paspalakis E 2021 *Sci. Rep.* **11** 1–11
[48] Asadpour S H and Faizabadi E 2022 *Appl. Opt.* **61** 8139–46
[49] Asadpour S H, Hamedi H R, Kirova T and Paspalakis E 2022 *Phys. Rev.* A **105** 043709
[50] Kadhim Z J, Alkaaby H H C, Izzat S E, Adhab A H, Dawood A H, Shams M A and Kadhim A A 2022 *Laser Phys. Lett.* **19** 105204
[51] Liu Y, Xiang Y and Mohammed A A 2022 *Laser Phys. Lett.* **19** 095205